



RESEARCH ARTICLE OPEN ACCESS

Prediction of Post Traumatic Epilepsy Using MR-Based Imaging Markers

Haleh Akrami¹ | Wenhui Cui¹ | Paul E. Kim² | Christianne N. Heck² | Andrei Irimia^{2,3}  | Karim Jerbi^{1,4,5} | Dileep Nair⁶ | Richard M. Leahy¹ | Anand A. Joshi¹ 

¹Department of Electrical and Computer Engineering, University of Southern California, Los Angeles, California, USA | ²Department of Radiology, University of Southern California, Los Angeles, California, USA | ³Leonard Davis School of Gerontology, University of Southern California, Los Angeles, California, USA | ⁴Psychology Department, Université de Montréal, Montreal, Quebec, Canada | ⁵Mila, Quebec AI Research Center, Montreal, Quebec, Canada | ⁶Epilepsy Center, Cleveland Clinic Neurological Institute, Cleveland, Ohio, USA

Correspondence: Anand A. Joshi (ajoshi@usc.edu)

Received: 4 March 2024 | **Revised:** 10 September 2024 | **Accepted:** 28 October 2024

Funding: This work was supported by National Institutes of Health, R01EB026299 Congressionally Directed Medical Research Programs, HT94252310149, W81XWH181061.

Keywords: fMRI | lesion detection | machine learning | MRI | PTE | TBI

ABSTRACT

Post-traumatic epilepsy (PTE) is a debilitating neurological disorder that develops after traumatic brain injury (TBI). Despite the high prevalence of PTE, current methods for predicting its occurrence remain limited. In this study, we aimed to identify imaging-based markers for the prediction of PTE using machine learning. Specifically, we examined three imaging features: Lesion volumes, resting-state fMRI-based measures of functional connectivity, and amplitude of low-frequency fluctuation (ALFF). We employed three machine-learning methods, namely, kernel support vector machine (KSVM), random forest, and an artificial neural network (NN), to develop predictive models. Our results showed that the KSVM classifier, with all three feature types as input, achieved the best prediction accuracy of 0.78 AUC (area under the receiver operating characteristic (ROC) curve) using nested cross-validation. Furthermore, we performed voxel-wise and lobe-wise group difference analyses to investigate the specific brain regions and features that the model found to be most helpful in distinguishing PTE from non-PTE populations. Our statistical analysis uncovered significant differences in bilateral temporal lobes and cerebellum between PTE and non-PTE groups. Overall, our findings demonstrate the complementary prognostic value of MR-based markers in PTE prediction and provide new insights into the underlying structural and functional alterations associated with PTE.

1 | Introduction

Traumatic brain injury (TBI) survivors often carry a tremendous burden of disability as a result of their injuries (Parikh, Koch, and Narayan 2007). Such injuries can have wide-ranging physical and psychological effects with some signs or symptoms that appear immediately after the traumatic event, while others appear days or weeks later. TBI is one of the major causes of epilepsy (Agrawal et al. 2006) yet the link between TBI and epilepsy is not fully understood. Post-traumatic epilepsy (PTE)

refers to recurrent and unprovoked post-traumatic seizures occurring after 1 week (Verellen and Cavazos 2010). Patients with PTE perform worse across several clinical and performance metrics such as independence and cognitive scores and have a significantly reduced quality of life (Burke et al. 2021). They are prone to higher rates of mental illness such as depression and addiction (Bushnik et al. 2012). Significant risk factors for the development of seizures > 1 week after TBI include seizures within the first week, acute intracerebral hematoma (especially subdural hematoma), brain contusion,

This is an open access article under the terms of the [Creative Commons Attribution](https://creativecommons.org/licenses/by/4.0/) License, which permits use, distribution and reproduction in any medium, provided the original work is properly cited.

© 2024 The Author(s). *Human Brain Mapping* published by Wiley Periodicals LLC.

increased injury severity, and age > 65 years at the time of injury (D'Ambrosio and Perucca 2004). The incidence of PTE ranges from 4% to 53%, with the risk approaching 50% in cases with direct injury to the brain parenchyma. PTE risk also varies with the time after injury, age range under study, as well as the spectrum of severity of the inciting injuries (D'Ambrosio and Perucca 2004; Frey 2003; Piccenna, Shears, and O'Brien 2017). Epidemiological studies have found that PTE accounts for 10%–20% of symptomatic epilepsies and 5% of all epilepsies (Herman 2002; Pitkänen and Bolkvadze 2012). It is estimated that in the United States and the European Union (EU), with a total population of about 800 million, at least 0.5 million surviving individuals live with PTE (Verellen and Cavazos 2010). Data on the economic burden of PTE are unavailable, but some idea is provided by the lifetime cost of TBI on average, which in the United States is around \$200,000 per case scaled to 2004 prices (Berg, Tagliaferri, and Servadei 2005; Humphreys et al. 2013). Thus, in addition to the personal burden, the economic burden caused by PTE is also substantial. Therefore, prediction and if possible, prevention of PTE remains an important challenge.

Biomarkers for PTE can vary from imaging and electrophysiologic measurements to changes in gene expression and metabolites in blood or tissues. MRI provides a non-invasive and powerful approach for marker development, without the use of ionizing radiation. While a wealth of biomarkers exists when the epilepsy condition is already established, these markers can only reveal mechanisms that exist after the epileptogenic process, which can allow partial or full pharmacoresistance to be established before treatment starts (Perucca 1998; Piccenna, Shears, and O'Brien 2017; Potschka and Brodie 2012). Prognostic markers and approaches to identify the risk of PTE would eliminate the need to wait for spontaneous epileptic seizures to occur before starting treatment. The ability to identify high-risk subjects can enable the mitigation of risks to subjects whose seizures could result in serious injury or death.

The pathogenesis of spontaneous recurrent seizures is certainly multifactorial. Once established, seizure threshold, which is a measure of the balance between excitatory (glutamatergic) and inhibitory (GABA-ergic) forces in the brain (Panayiotopoulos 2005; Sackeim et al. 1987), is thought to vary over time depending on several factors such as periodicities in seizure occurrence (Baud et al. 2018). Current anti-seizure medications raise the seizure threshold and thus reduce the propensity for seizures to occur. An individualized prognostic marker for the development of PTE could be used in clinical trials to study compounds that may have true anti-epileptic potential. Current medications used for epilepsy only treat the symptoms, not the underlying pathophysiology that leads to epilepsy. The value of individualized prognostic markers is fivefold (Engel Jr et al. 2013). (i) Prediction of the development of an epilepsy condition: Prognostic markers that eliminate the need to wait for spontaneous epileptic seizures to occur would reduce the time and cost required for TBI patients to start participation in clinical trials, and also the risks to subjects whose seizures could result in serious injury or death. (ii) Identification of the presence and severity of tissue capable of generating spontaneous seizures: An imaging-based marker can identify anomalous brain regions; which could help in surgical as well as noninvasive

treatment planning even before the condition is established. (iii) Measuring progression after the condition is established: MR imaging-based markers can help in quantifying the progression of epilepsy and understanding pharmacoresistance. Identification of localized biomarkers of epileptogenic brain abnormalities would allow longitudinal tracking of seizure threshold at later time points and would presumably reveal the time points when the epileptogenic process reaches a critical point so that clinical seizures would likely occur. (iv) Creating animal models of PTE: The identified markers can be used to create animal models, and prediction algorithms can be used for more cost-effective screening of animal models for treatment with potential anti-epileptogenic and antiseizure drugs and devices. (v) Cost reduction in clinical trials by screening patients: PTE risk prediction can be used for recruitment into clinical trials for potential anti-epileptogenic interventions by enriching the trial population with identified patients who are at higher risk for developing epilepsy.

Prediction and if possible, prevention of the development of PTE is a major unmet challenge. Animal studies in adult male Sprague–Dawley rats have shown the potential of using MRI-based image analysis for finding biomarkers for PTE (R. Immonen et al. 2013; Pitkänen et al. 2016). These studies point toward the involvement of the perilesional cortex, hippocampus, and temporal lobe in PTE (Pitkänen and Bolkvadze 2012). Despite important progress, brain imaging is still underexploited in the context of PTE biomarker research. Numerous human neuroimaging studies have provided important insights into TBI (Dennis et al. 2016; Farbota et al. 2012; Kim et al. 2008) and epilepsy (W. Li et al. 2009; Mo et al. 2019; Sollee et al. 2022), but imaging-based PTE prediction work is scarce.

Group analyses of TBI patients compared to controls revealed volume reductions in several brain regions, including cortical areas like the cingulate gyrus, precuneus, and parahippocampal gyrus (Farbota et al. 2012; Gale et al. 2005; Kim et al. 2008; Sidaros et al. 2009; Yount et al. 2002). Additionally, reductions were observed in white matter structures, including the corpus callosum and corona radiata, as well as subcortical regions like the hippocampus, amygdala, putamen, globus pallidus, caudate, and midbrain (Dennis et al. 2016; Farbota et al. 2012; Gale et al. 2005; Sidaros et al. 2009; Tasker et al. 2005; Wilde et al. 2007).

Clinical and research studies in epilepsy often include both anatomical (MRI and CT) and functional (PET, EEG, MEG, ECoG, depth electrodes, and fMRI) mapping. While epileptogenic zones can be found in almost any location in the brain, the temporal lobe and the hippocampus are the most common sites causing focal epileptic seizures (Sollee et al. 2022). Multimodal MRI and PET imaging have been used to predict the laterality of temporal lobe epilepsy (Pustina et al. 2015; Sollee et al. 2022). Extensive changes in brain networks due to epilepsy were reported using PET, fMRI, and diffusion imaging (W. Li et al. 2009; Pitkänen et al. 2016; Pustina et al. 2015; Akrami et al. 2021; Sollee et al. 2022).

Research using resting-state fMRI (rs-fMRI) over the last two decades has uncovered important properties of brain dynamics and network organization by revealing the existence

of patterns of spontaneous neural activity that occur in the absence of a specific task or stimulus. These patterns, known as resting-state networks, have been found to be consistent across individuals and are thought to reflect the underlying functional organization of the brain (Arslan et al. 2018). The presence of lesions in TBI patients is expected to alter these resting-state brain dynamics either locally, through changes in the lesioned area, or at the level of networks affected by the lesion (Palacios et al. 2013). In addition, previous work has shown that cases of focal epilepsy are often associated with changes in network activity extending beyond the seizure onset zone (Yamazoe et al. 2019; Pedersen et al. 2015). Interestingly, Zhou et al. (2020) trained a support vector machine (SVM) classifier on brain imaging data for the diagnosis of mesial temporal lobe epilepsy, and found that combining fMRI and structural MRI features provided better classification than either modality alone. Taken together, these studies motivate the exploration of local and network-level brain abnormalities as potential predictive markers of PTE in patients who have suffered from a TBI.

A few recent studies have employed machine learning to identify functional brain changes that may serve as PTE biomarkers (Rocca et al. 2019; Akrami et al. 2021; Cui et al. 2023). Common features used in such brain-based prediction approaches are the pair-wise correlation patterns observed between rs-fMRI signals. However, because of the high dimensionality of such connectivity metrics, using them as features in a machine-learning framework can quickly lead to model overfitting. A standard approach to dealing with this issue is to use a dimensionality reduction method such as principal components analysis (PCA) to reduce the dimension of the feature space to a subset of principal components that represents nevertheless most of the information in the data. Moreover, regularized models (Hastie, Tibshirani, and Friedman 2001; Toloși and Lengauer 2011) with a ridge or lasso penalty can also be used to select a subset of features and prevent overfitting by penalizing the weights. In the specific case of exploiting brain connectivity features in a dataset with a limited number of subjects, the presence of groups of highly correlated features leads to an ill-conditioned feature space. As a result, methods that use simple penalties that discard most of the correlated features can become unstable (Toloși and Lengauer 2011).

The goal of the present study was to probe the utility of multiple structural and functional features extracted from MR imaging in characterizing PTE, as well as predicting its occurrence. We explored both classical group-level statistics and cross-validated machine-learning methods. Our main hypothesis is that we will find biomarkers for PTE in anatomical and functional maps. Furthermore, we hypothesize that MRI-derived features can be used to predict PTE on an individual basis. Our working hypothesis is that we will find markers for PTE within the TBI population that will be a combination of (a) the lesion features, detected automatically using a machine-learning method and (b) local resting functional connectivity-based features. We expect to find regions and networks indicating a higher chance that the subject is predisposed to developing PTE, including the cerebellum, temporal lobe, frontal lobe, hippocampus, and thalamus. Our results

extend previous reports by uncovering key MR-based differences between TBI patients who develop PTE and those who do not. In addition, we were able to leverage machine learning analyses to assess the relative contribution of different types of structural and functional features to the out-of-sample prediction of PTE.

2 | Materials And Methods

2.1 | Data

We extracted functional and structural features from two datasets:

1. The Maryland TBI MagNeTs dataset (Gullapalli 2011): Of the 113 individual datasets, 72 (36 PTE and 36 non-PTE groups) were used for group-level difference comparisons as well as for supervised training and testing of a machine-learning algorithm (i.e., constructing a model from training samples to predict the presence of PTE in previously unseen data). The remaining 41 non-PTE subjects (a total of 113) were used to train an artificial neural network for automatic lesion delineation, using a method recently developed by our group (Akrami et al. 2020).
2. The TRACK-TBI Pilot dataset (Yue et al. 2013): 97 subjects from this dataset, in addition to the 41 non-PTE subjects from MagNeTs, were used to train the artificial neural network for automated delineation of lesions as described briefly below in Section 2.2.2. A more detailed description can be found in (Akrami et al. 2020).

2.1.1 | Maryland MagNeTs Data

This is our main dataset for group comparisons as well as for PTE prediction. The dataset was collected as a part of a prospective study that includes longitudinal imaging and behavioral data from TBI patients with Glasgow Coma Scores (GCS) in the range of 3–15 (mild to severe TBI). Injury mechanisms included falls, bicycle or sports accidents, motor vehicle collisions, and assaults. The individual or group-wise GCS, injury mechanisms, and clinical information is not shared. The imaging data are available from FITBIR (<https://fitbir.nih.gov>), with FLAIR, T_1 , T_2 , fMRI, diffusion, and other modalities available for download. In this study, we used imaging data acquired within 10 days after injury, and seizure information was recorded using follow-up appointment questionnaires. Exclusion criteria included a history of white matter disease or neurodegenerative disorders including multiple sclerosis, Huntington's disease, Alzheimer's disease, Pick's disease, and a history of stroke or brain tumors.

The imaging was performed on a 3T Siemens TIM Trio scanner (Siemens Medical Solutions, Erlangen, Germany) using a 12-channel receiver-only head coil. For statistical analysis, we used 36 fMRI subjects with PTE (25M/11F) from this dataset and 36 randomly selected fMRI subjects without PTE (28M/8F) (Gullapalli 2011; Y. Zhou et al. 2012). The age range for the epilepsy group was 19–65 and 18–70 years for

the non-epilepsy group. Our analysis of population differences was performed using T_1 -weighted, T_2 -weighted, and FLAIR MRI as well as resting fMRI (Gullapalli 2011). The remaining 41 subjects with TBI but without PTE were used for training the automatic lesion detection algorithm. Standard gradient-echo echo-planar resting-state functional MR imaging (repetition time ms/echo time ms, 2000/30; flip angle, 75°; field of view, 220×220 mm; matrix, 128×128; 153 volumes) was performed in the axial plane, parallel to a line through the anterior and posterior commissures (section thickness, 5 mm; section gap, 1 mm) and positioned to cover the entire cerebrum (spatial resolution, 1.72×1.72×6.00 mm) with an acquisition time of 5 min 6 s. The individuals were instructed to close their eyes for better relaxation but to stay awake during the imaging protocol.

2.1.2 | TRACK-TBI Pilot Dataset

This is a multi-site study with data across the injury spectrum, along with CT/MRI, blood biospecimens, and detailed clinical outcomes (Yue et al. 2013). Here, we use 3T MRI data in addition to information collected according to the 26 core Common Data Elements (CDEs) standard developed by the TrackTBI Neuroimaging Working Group (Meeuws et al. 2020). The 3T MRI protocols (implemented on systems from General Electric, Phillips, and Siemens) complemented those used in the Alzheimer's Disease Neuroimaging Initiative (ADNI) with $T_R/T_E = 2200/2.96$ ms, an effective T_1 of 880 ms, an echo spacing time of 7.1 ms, a bandwidth 240 Hz/pixel, and a total scan time of 4 min and 56 s. The data are available for download from <https://fitbir.nih.gov>.

To train the unsupervised deep learning model, a variational auto-encoder for lesion delineation as described in Section 2.2.2, we used 2D slices of brain MRIs from a combined group of 41 TBI subjects (33 M/8 F, age range 18–82 years) from the Maryland TBI MagNeTs study (Gullapalli 2011) and 97 TBI subjects (70 M/27 F, age range 11–73 years) from the TRACK-TBI Pilot study (Yue et al. 2013). These TBI data were taken from patients without PTE, and are strictly distinct from the set of 72 subjects which we subsequently used for statistical testing and PTE prediction.

2.2 | Methods

2.2.1 | Preprocessing

Pre-processing of the MR datasets was performed using the BrainSuite software (<https://brainsuite.org>) (Shattuck and Leahy 2002). The three modalities (T_1 , T_2 , and FLAIR) were coregistered with each other by registering T_2 and FLAIR to T_1 , and the result was co-registered to the MNI atlas (Colin 27 Average Brain) (Collins et al. 1995) by registering T_1 images to the MNI atlas using a rigid (translation, scaling, and rotation) transformation model. As a result, all three image modalities were registered to a common MNI space at 1 mm³ resolution. Skull and other non-brain tissue were removed using BrainSuite (Joshi et al. 2018), and brain extraction was performed by stripping away the skull, scalp, and any non-brain tissue from the image. This was followed by tissue classification and generation

of the inner and pial cortex surfaces. Subsequently, for training and validation of the lesion detection model, all images were reshaped into 128×128 pixel images and histogram-equalized to a lesion-free subject.

The extracted cortical surface representations and brain image volumes for each subject were jointly registered to the BCI-DNI Brain Atlas (http://brainsuite.org/svreg_atlas_description/) (Joshi et al. 2022) using BrainSuite's Surface-Volume Registration (SVReg18a) module (Joshi et al. 2007, 2005). The BCI-DNI brain atlas is from a single subject with parcellation defined by anatomical landmarks. SVReg uses anatomical information from both the surface and volume of the brain for accurate automated co-registration, which allows consistent surface and volume mapping to a labeled atlas. This co-registration establishes a one-to-one correspondence between individual subjects' T_1 MRIs and the BCI-DNI brain atlas. The deformation map between the subject and the atlas encodes the deformation field that transforms images between the subject and the atlas.

We used the BrainSuite fMRI Pipeline (BFP) to process the rs-fMRI subject data and generated grayordinate representations of the preprocessed rs-fMRI signals (Glasser et al. 2013). BFP is a software workflow that processes fMRI and T_1 -weighted MR data using a combination of software that includes BrainSuite, AFNI (Cox 2012), FSL (Jenkinson et al. 2012), and MATLAB scripts to produce processed fMRI data represented in a common grayordinate system that contains both cortical surface vertices and subcortical volume voxels. Starting from raw T_1 and fMRI images, BFP produces processed fMRI data co-registered with BrainSuite's BCI-DNI atlas and includes both volumetric and grayordinate representations of the data.

2.2.2 | MRI-Based Measures: Lesion Detection

We used multimodal MRI images (T_1 , T_2 , and FLAIR) pre-processed using steps described in Section 2.2.1. These images were skull-stripped, co-registered to MNI atlas and resampled at 1 mm³ resolution. To extract lesions from the anatomical MRI data we used an unsupervised framework which we recently developed to automatically detect lesions in MR data. The method, which has been validated on other datasets, is based on a variational auto-encoder (VAE), a class of auto-encoders where the latent representation can be used as a generative model (Chen and Konukoglu 2018; Kingma and Welling 2013; Akrami et al. 2022b). By training the VAE using nominally healthy (lesion-free) imaging data, the network learns to encode normal brain images. As a result, applying such a model to an image that contains a lesion will yield a VAE-decoded image that does not contain anomalies: The lesions can then be identified from the differences between original and VAE-decoded images. One complication here is that we did not have access to normal imaging data with matching characteristics of the PTE dataset. Instead, we trained VAE using the T_1 -weighted, T_2 -weighted, and FLAIR MRIs in the Maryland TBI MagNeTs dataset (Gullapalli 2011) leveraging VAEs robustness to outliers (Akrami, Joshi, et al. 2022). While lesions are present in most of the volumetric TBI images, they are typically confined to a limited region in each brain, so that in any particular anatomical region (at the scale of the major gyri delineated in the BCI-DNI

atlas) the fraction of images with lesions is relatively low. In this study, the lesions were delineated based on VAE reconstruction error in the FLAIR images. We utilized the VAE architecture proposed in (Akrami et al. 2020), which features an encoder composed of three consecutive blocks. Each block consists of a convolutional layer, a batch normalization layer, a ReLU activation function, and two fully connected layers in the bottleneck. The decoder includes a fully connected layer followed by three consecutive blocks of deconvolutional layers, each with batch normalization and ReLU, and a final deconvolutional layer. After generating the reconstruction error map, a median filter of size 7×7 was applied to remove isolated pixels. We have previously evaluated the performance of this lesion detection algorithm using an independent validation set with delineated lesions (Akrami et al. 2020, Akrami, Leahy, Irimia, et al. 2022).

Statistical analyses: Once we determined the lesions using the methods described above, we analyzed the VAE lesion maps using a 1-sided nonparameteric (permutation-based) F-test to determine whether there were any statistically significant differences in the variances of lesion maps across the PTE and non-PTE TBI groups (Akrami, Leahy, Irimia, et al. 2022). The null hypothesis is that the variances of lesion maps across subjects in the PTE group is less than or equal to that of the non-PTE group. Our decision to use the F-test was guided by the fact that traumatic brain injuries affect different areas in different subjects across the groups, so that consistently localized differences between the two groups were expected to be very unlikely. However, a higher frequency of lesions in a particular region should result in a higher sample variance in the lesion maps. This rationale was in fact supported by our observation that assessing differences in the group means using a standard t-test did not show any significant effects. To apply an F-test with permutations, we computed point-wise group variances and computed their ratio to obtain an unpermuted F-statistic. We then permuted the group labels to recompute the F-statistic for $nperm = 1000$ permutations. The p value was computed pointwise by comparing the unpermuted F-statistic to the permuted F-statistics ($nperm = 1000$). Finally, the resulting pointwise map of p values was corrected for multiple comparisons using false discovery rate (FDR) correction (Benjamini and Hochberg 1995). While this procedure does not explicitly account for voxel correlations, it allows for positive correlations among voxels, making it suitable for image-based analyses commonly used in neuroimaging (Genovese, Lazar, and Nichols 2002).

Additionally, we performed a regional analysis by quantifying lesion volume from binarized lesion maps in each ROI using the USCLobes brain atlas (Joshi et al. 2022) (Lobe-wise analysis) (<http://brainsuite.org/usclobes-description>). The USCLobes atlas segments the brain into larger regions (lobes) than those provided by the default BrainSuite atlases. It has 15 ROIs delineated on the volumetric labels of the atlas: (L/R) Frontal Lobe, (L/R) Parietal Lobe, (L/R) Temporal Lobe, (L/R) Occipital Lobe, (L/R) Insula, (L/R) Cingulate, Brainstem, Cerebellum, and Corpus Callosum. The subject MRIs were preprocessed and parcellated into lobes using the USCLobes atlas as described in Section 2.2.1. The lesion volume per lobe was computed for each subject using the USCLobes parcellation (Joshi et al. 2022). For each lobe, the lesion volumes were compared PTE and non-PTE group using ranksum test (Mann and Whitney 1947). The

null hypothesis was that the lesion volume in the PTE group was less than or equal to the lesion volume in the non-PTE group. Multiple comparisons across the regions were accounted for using the Benjamini–Hochberg procedure (Benjamini and Hochberg 1995).

To identify lesions as binary masks, a one-class SVM (Zhang et al. 2004) was applied to the VAE lesion maps at each voxel and across subjects to identify subjects with abnormally large errors (i.e., discrepancies between the original input image and VAE-decoded image) at that voxel (Zhang et al. 2004; Duda, Hart, and Stork 2012). We defined the outliers marked by the one-class SVM as lesions and computed lesion volumes per ROI by counting the number of outlier voxels in each ROI for each subject. In the following, we consider this measure to be a proxy for an ROI-wise lesion volume, which we use for PTE prediction.

2.2.3 | fMRI Based Measures: Connectivity

We compute ROI-wise connectivity using rs-fMRI data and the USCLobes ROIs. The BFP fMRI pipeline produces a standardized fMRI signal in the grayordinate system that is in point-wise correspondence across subjects. Using the USCLobes parcellation with respect to the grayordinates, we computed the ROI-wise signal by averaging over each ROI. A 15×15 matrix was then computed from the Pearson correlations of averaged fMRI signals between each of the 15 ROIs in the USCLobes atlas. We used the elements of the upper triangle of the correlation matrix as a feature vector and applied the Fisher z transform to normalize the feature distribution. This feature vector was subsequently used for classification.

2.2.4 | fMRI-Based Measures: ALFF

The ALFF (Zuo et al. 2010; Wang et al. 2019) is an rs-fMRI-based metric that measures the magnitude of spontaneous fluctuations in BOLD-fMRI signal intensity for a given region. We calculated the ALFF metric (Wang et al. 2019) as the signal power in a frequency band defined by a low- and high-frequency cutoff, which we set to 0.01 and 0.1 Hz, respectively. The ALFF measure was first computed in the native fMRI space and then mapped to the mid-cortical surface of the USCBrain atlas (Joshi et al. 2022) using the BrainSuite registration method described above.

Statistical analyses: Similar to the statistical assessment of lesion differences, we used a 1-sided F-test (null hypothesis var. in PTE \leq var. in nonPTE populations). We tested for significance using a permutation method ($nperm = 1000$), for voxel-wise group-level comparison of variance across the PTE and non-PTE groups. These resulting p values were corrected for multiple comparisons using the FDR (Benjamini Hochberg procedure) (Benjamini and Hochberg 1995). As a result, we end up with a voxelwise p value map in the USCBrain atlas space, indicating local differences in slow-frequency fluctuations of BOLD between PTE and non-PTE groups.

In addition to the voxel-wise analysis, we also performed lobe-wise analysis, similar to Section 2.2.2. The subject MRIs were preprocessed and parcellated into lobes using the USCLobes

atlas as described in Section 2.2.1. The average ALFF over each lobe was computed for each subject using the USCLobes parcellation (Joshi et al. 2022). For each lobar region, the average ALFF scores were compared to PTE and non-PTE groups using the F-test. The null hypothesis was that the variance of ALFF in the PTE group was less than or equal to the variance of ALFF in the non-PTE group. Multiple comparisons across the regions were accounted for using the Benjamini–Hochberg procedure (Benjamini and Hochberg 1995).

2.2.5 | PTE Prediction Using Machine Learning

In addition to the statistical analyses described above, we examined the same brain features using a supervised machine-learning framework (Akrami et al. 2021). This was motivated by several factors. The machine-learning framework allows us to implement an out-of-sample analysis that assesses the ability of the features extracted from the data to classify individual subjects. This is particularly important when searching for potential biomarkers. Second, tools such as multi-feature classification and feature importance quantification readily provide useful insights into the significance, complementarity, or redundancy across the set of explored features. This is also key when seeking to identify the most efficient prognostic biomarkers. Finally, the diversity of available machine-learning algorithms opens novel opportunities to tease apart variable distributions that may be harder to separate using standard statistical tools.

In the machine-learning pipeline implemented in the present study, we used the anatomical and functional features described above (i.e., lesion information, connectivity, and ALFF) that were extracted from MR imaging data collected during the early (acute) phase prior to the onset of PTE. The goal of the data-driven classifier approach is to build a model that learns to distinguish between PTE and non-PTE subjects using labeled training data. We use a leave-one-out stratified cross-validation scheme to reduce risks of selection bias and overfitting. To fine-tune model hyperparameters while adhering to a strict separation of training and test data, we used a standard nested cross-validation procedure.

To assess the feasibility of building models that can predict PTE from structural and functional MR data, we implemented a multi-feature binary classification framework using three distinct types of algorithms (details below). We concatenated the extracted features into an input vector, to which we applied PCA to reduce the dimensionality of the feature space (Dunteman 1989; Ringnér 2008). We use the area under the receiver operating characteristic curve (AUC) as the primary performance evaluation metric.

We applied the following three machine-learning algorithms:

Random Forests (Breiman 2001): We used a random forest classifier which is an ensemble learning method that works by training multiple decision trees on random subsets of the data and then averaging the predictions of each tree to make a final prediction. This technique reduces overfitting and improves the overall accuracy of the model compared to using a single decision tree. At each iteration, a random subsample of the data is

taken, and a new decision tree is fit. This process is repeated multiple times, and the final output is the majority vote of all the decision trees.

SVMs and Kernel-SVMs (KSVMs): The basic idea underlying the SVM is to find the hyperplane in a high-dimensional space that maximally separates the different classes (Cortes and Vapnik 1995). The data points that are closest to the hyperplane are called support vectors and have the greatest impact on the position of the hyperplane. Once the hyperplane is found, new data can be easily classified by determining on which side of the hyperplane they fall. By contrast, a KSVM, is an extension of the basic SVM algorithm that uses a kernel operator to map the input data into a higher-dimensional space, in which they can be more easily separated. The use of a kernel allows the SVM to handle non-linearly separable data by finding a higher-dimensional space in which they are linearly separable. One of the most popular kernels for this purpose, and that used here, is the radial basis function (RBF).

Multi-Layer Perceptron: We also used a multilayer perceptron (MLP) which is a feedforward artificial neural network where the input is passed through multiple layers of artificial neurons. Each layer applies a non-linear transformation to the input before passing to the next layer (X. Li et al. 2019). MLPs are trained using back-propagation and stochastic gradient descent. The MLP model we used here consisted of three hidden layers (32, 16, and 16 neurons, respectively). While more complex and deeper neural network architectures are available, we chose to use a simple MLP given the limited size of the data at hand ($N=72$). We expected the RF and SVM algorithms to be more suitable for our classification task, but included the MLP method for the sake of comparison.

3 | Results

3.1 | Lesion Analysis

To compare lesion patterns across the PTE and non-PTE patients, we assessed group differences in lesion scores, defined as the difference between the grayscale values in the original anatomical MR images and the VAE-decoded versions thereof (see methods). Statistical assessment using the F-test revealed statistically significant differences ($p < 0.05$, corrected) between the two groups in multiple brain areas (Figure 1). These differences were prominent in the left and right temporal lobes, the right occipital lobe, and the cerebellum, reflecting higher variability of lesion scores in these areas in PTE patients.

Our lobe-wise analysis (Table 1) yielded results consistent with voxel-wise analysis, confirming an increased variance in the PTE population relative to non-PTE subjects in the same regions identified in the grayordinate-wise analysis.

3.2 | PTE-Related Modulations of ALFF

A point-wise group difference analysis of ALFF is shown in Figure 2. The results of the lobar analysis of ALFF (Table 1) are consistent with the grayordinate-wise analysis (Figure 1), both

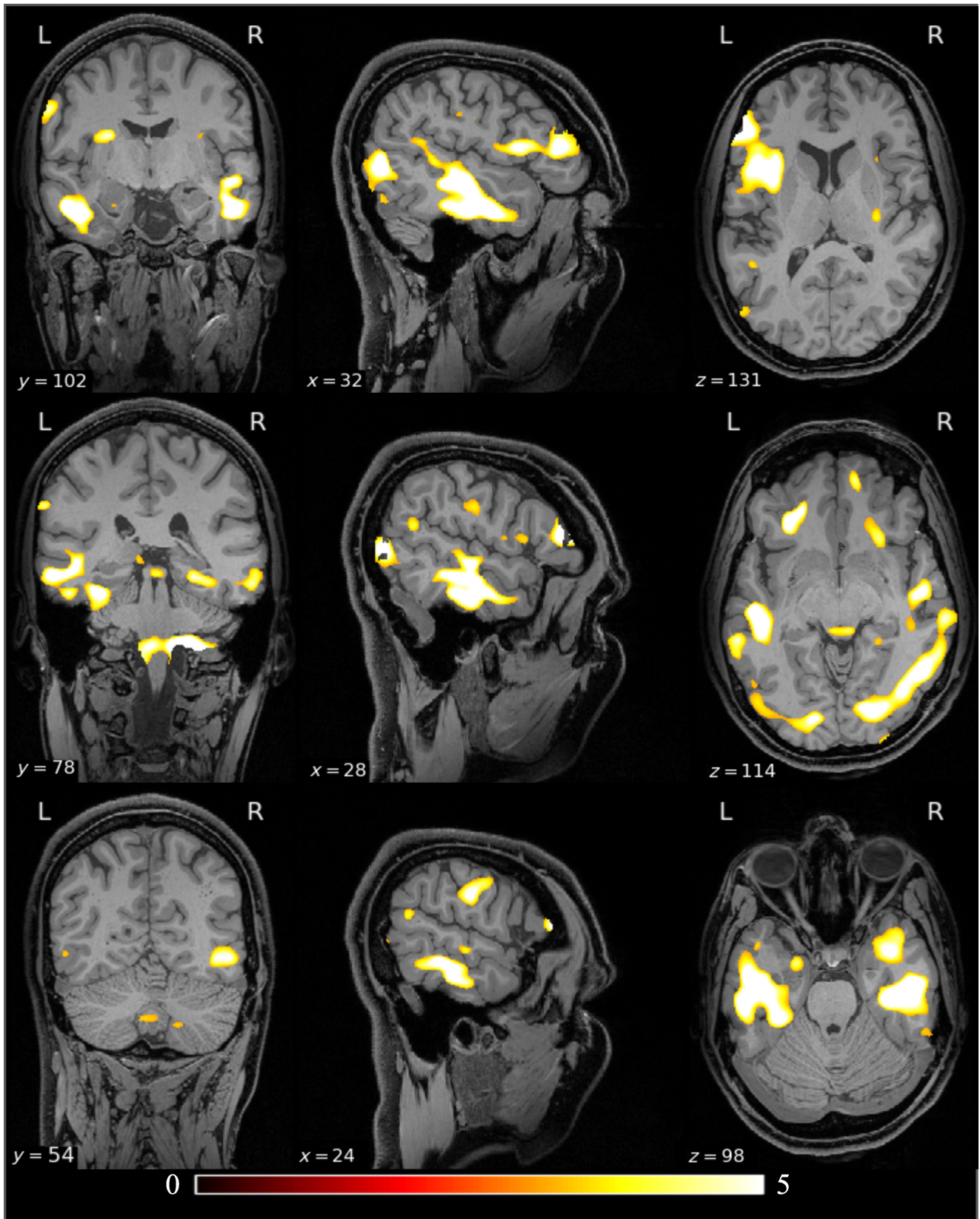


FIGURE 1 | Voxel-based PTE versus non-PTE group comparison of lesion maps overlaid on the USCBrain atlas. The color code depicts F-values, shown in a region where p value < 0.05 , resulting from the F-test (with permutations). Prominent significant clusters are located in the left temporal lobe, bilateral occipital lobe, cerebellum, and right parietal lobe. The un-thresholded maps of F-values for the lesion comparisons are shown in the Figure S1.

TABLE 1 | Classification accuracy of PTE versus non-PTE subjects using different classifiers and feature types.

Method	Lesion	Connectivity	ALFF	Combined
KSVM	0.55 (0.04)	0.61 (0.07)	0.62 (0.04)	0.78 (0.04)
SVM	0.63 (0.03)	0.51 (0.04)	0.63 (0.02)	0.64 (0.03)
RF	0.58 (0.05)	0.55 (0.08)	0.67 (0.03)	0.64 (0.06)
NN	0.50 (0.04)	0.61 (0.08)	0.50 (0.05)	0.56 (0.02)

Note: The mean and standard deviation of AUC are shown for KSVM, SVM, RF, and NN. The last column shows the performance obtained when the models were trained simultaneously on all three feature types.

showing an increased variance in the PTE population relative to non-PTE subjects in the right temporal lobe, both occipital lobes, right parietal lobe. The asymmetry in the lobe-based analysis is possibly due to the limited sample size.

The glass brain renderings of F-values for lesion and ALFF comparisons of PTE versus non-PTE groups are shown in Figure 3. The unthresholded F-value maps of lesion and ALFF comparisons are shown in the (Figures S1,S2). The lesion comparison shows significantly higher F-values compared to the ALFF comparison, indicating that at early stages of TBI, lesion distribution is a stronger focal predictor of PTE relative to ALFF.

3.3 | Classification of PTE and Non-PTE Subjects Using Machine Learning

To test the feasibility of training an ML model to distinguish PTE and non-PTE data, we performed leave-one-pair-out nested stratified cross-validation over 1000 iterations. Nesting was used for parameter tuning (the number of PCA components and model hyperparameter). Single-feature classification using either the lesion, connectivity, or ALFF metrics was followed by a multi-feature classification approach combining all three features. The input features were computed for distinct ROIs, based on the USCLobes atlas, and were normalized to unit variance, zero mean. From Table 2, we can see that combining all three feature types yields the best model performance in terms of the AUC scores. This is likely a reflection of the complementarity of the information about PTE captured across the lesion, connectivity, and ALFF data. Among the four ML methods we used, KSVM achieved the best performance. This is probably due to high variability in the feature space and improved feature separation through mapping to a higher dimensional space. The neural network performed relatively poorly on this classification, which given the moderate training sample size, is not surprising.

To check the significance of the AUC values, and to compare the performance of the ML methods to “chance” level classification, we performed permutation tests for all the classifiers by randomly permuting the subject labels at each of the 1000 cross-validation folds. A null distribution of AUC computed for chance level is shown in Figure 4. The distribution of AUCs was estimated using kernel density estimation from the histograms for the null AUC and the AUC for KSVM using all the features. We performed the rank-sum test to rule out the null hypothesis that the AUC null has the same mean as the AUC for the unpermuted classification. The *p* value for the classifier was below

the numerical precision, supporting the claim that this AUC is significantly better than the AUC that could be obtained by random chance.

In addition to determining the feature space based on the USCLobes atlas, we also computed ROI-based features using atlases with a large number of parcels. To this end we used the USCBrain atlas, BCI-DNI atlas (Joshi et al. 2022), and AAL3 atlas (Rolls et al. 2020). Running the classification pipeline based on these atlases did not lead to any significant improvements in PTE prediction.

To gain further insights and improve the interpretability of these ML results, we sought to assess the distinct spatial contributions of the lesion features to the overall prediction score. To this end, we computed feature importance maps derived from the positive SVM model coefficients. Figure 5 shows the lesion variability maps (in non-PTE and PTE subjects), followed by the SVM feature importances across the USCBrain atlas. Comparison between the lesion and feature importance maps points toward a reasonable spatial overlap between the two. But, most importantly, this analysis suggests that the lesion volume data that contribute most to distinguishing PTE and non-PTE subjects are located in the right temporal and left prefrontal cortices. Additionally, in the supplemental material (Figures S3 and S4), we also show the corresponding SVM feature importance maps for USCLobes and Brainnetome atlases (Joshi et al. 2022; Fan et al. 2016), which have lower and higher density parcellations compared to USCBrain atlas. These maps show a similar regional distribution of feature importance for PTE versus non-PTE classification.

4 | Discussion

The complex pathophysiology as well as the variability in the degree of severity of TBI poses a significant challenge to any research in this field. TBI with the resultant coup, focal cortical injury, and contrecoup injury, secondary contusion opposite to the coup injury, results in a great variety of cortical lesion sites, which then gives rise to a diversity of neurocognitive impairments (Ng and Lee 2019). The cortical injury inflicted by TBI is well known to have some predilection to the polar regions of the brain, particularly the temporal and frontal lobes (Fordington and Manford 2020). This is related to adjacency to the bony structures of the skull. However, the presence of cortical lesions in specific regions has not been consistently linked to the development of PTE. In one study, a left parietal lobe lesion and the presence of hemosiderin staining were

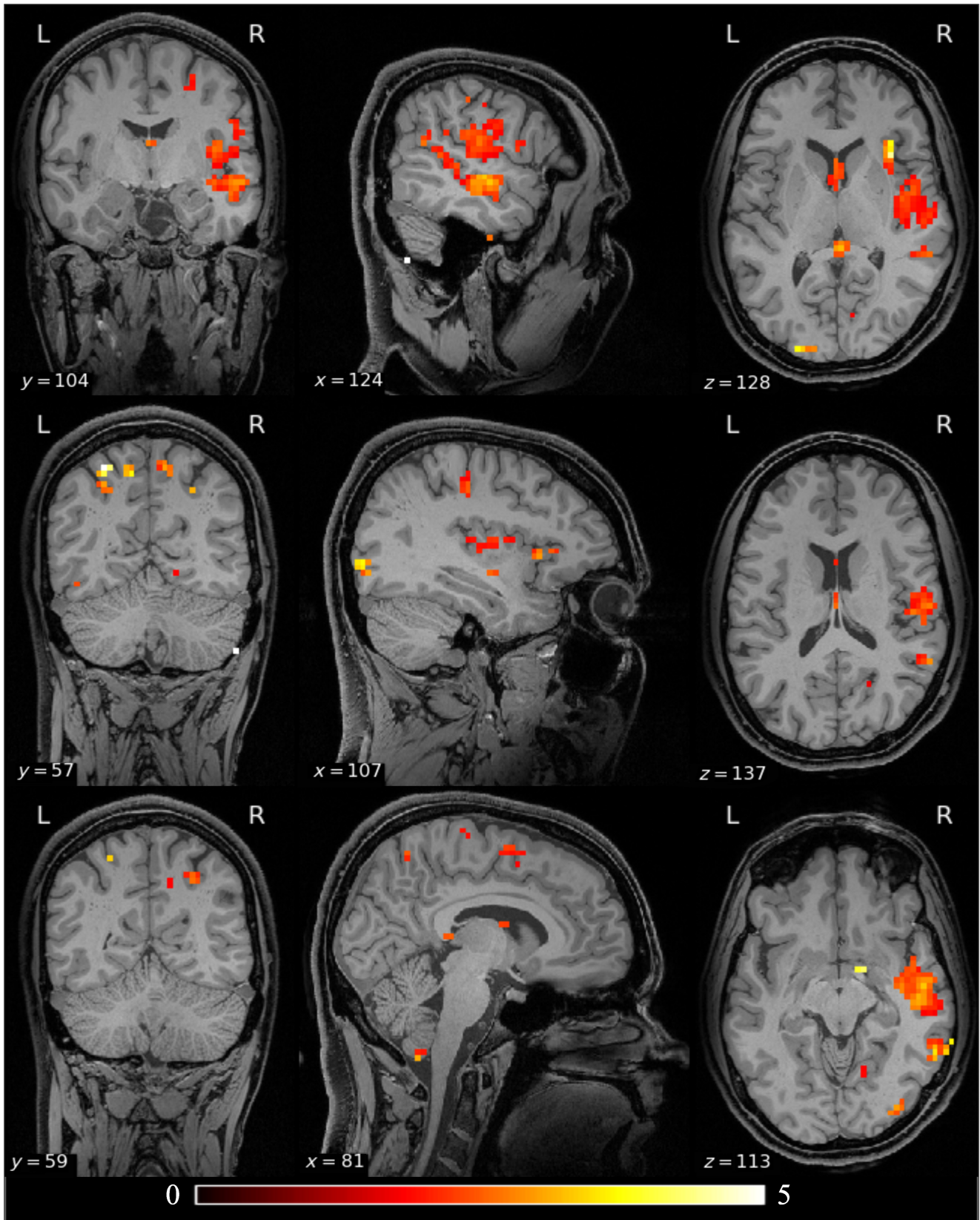


FIGURE 2 | Differences in ALFF between the PTE and non-PTE groups. The results are color-coded F-statistic thresholded by FDR-corrected p values ($p < 0.05$) derived using a permutation test. Significant clusters are visible in the left temporal lobe, bilateral occipital lobes, cerebellum, and right parietal lobe. The un-thresholded maps of F-values for the ALFF comparisons are shown in the Figure S2.

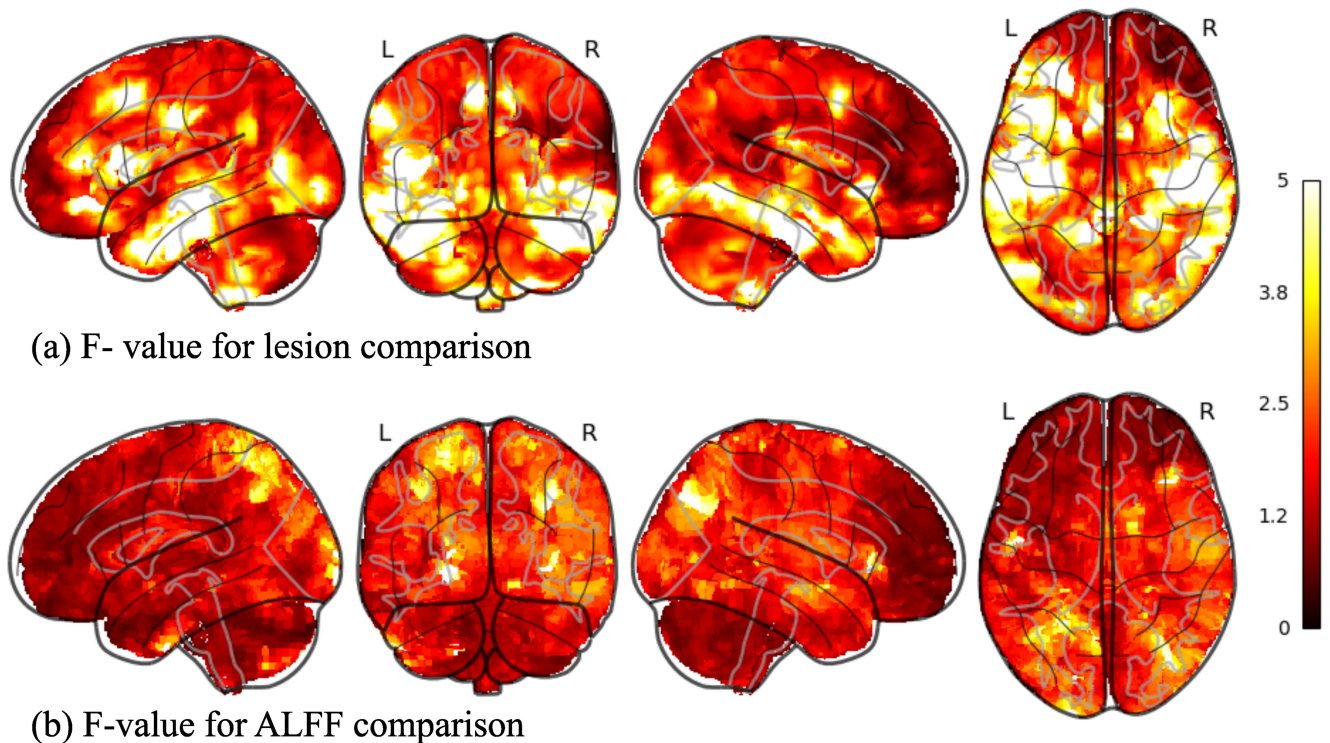


FIGURE 3 | (a) Glass brain rendering of the F- value for lesion comparison between PTE and non-PTE. (b) Glass brain rendering of the F-value for ALFF comparison between PTE and non-PTE. The higher F-values in lesions compared to ALFF comparisons show that lesions could be a stronger focal marker of PTE compared to functional changes at an early stage after TBI.

TABLE 2 | PTE versus non-PTE group comparison of lesion and ALFF measures (p values obtained using an F-test).

Lobe	p value (lesion) permutation test	p value (ALFF) permutation test
Right temporal	0.010	0.003
Left temporal	0.021	0.081
Right occipital	0.031	0.035
Left occipital	0.127	0.009
Right frontal	0.221	0.243
Left frontal	0.326	0.177
Right parietal	0.574	0.003
Left parietal	0.654	0.069
Right insula	0.347	0.226
Left insula	0.546	0.724
Cerebellum	0.047	0.072

Note: Bold values denote statistically significant ($p < 0.05$).

linked to the development of PTE (Raymont et al. 2010). Yet in other studies, rather than a specific cortical region, the degree of leakage by the blood–brain barrier around cortical sites after TBI was a prognostic marker for the development of PTE (Pitkänen et al. 2016). Due to the extreme heterogeneity of PTE, the need for a reliable biomarker to enhance the prediction of PTE is highly desirable. There have been a number of promising and novel therapeutic interventions targeting the complex pathophysiology of TBI shown to have promise in preclinical phase I/II trial, yet have gone on to fail in phase

III clinical trials (Ng and Lee 2019). Some reasons for failure could be the large sample required to determine benefit if the effect size of the intervention is small. The use of biomarkers could enrich the target population so as to maximize the likelihood of the discovery of potential therapeutic intervention.

Previous imaging studies that have studied epileptogenesis have shown that the progression of pathology has different temporal courses in the cortex and hippocampus (R. J. Immonen et al. 2009). Long-term alterations of the brain

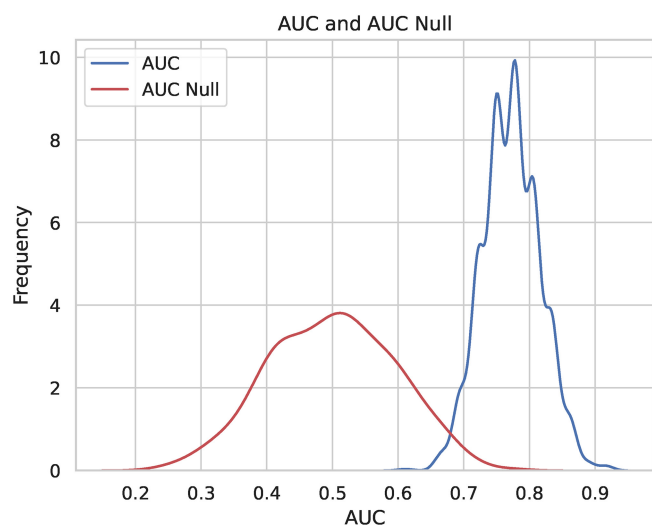


FIGURE 4 | The distribution of AUC computed for the random chance classifier and the KSVM classifier with all the features is computed using a permutation test. The ranksum test showed that the two classifiers have significantly different AUCs.

involve neuronal loss, white matter injury, and altered cerebral blood flow as well as metabolism. The data available from human studies have shown evidence for hippocampal neurodegeneration and mossy fiber sprouting (Swartz et al. 2006). As a result, about half of patients with PTE develop mesial temporal lobe sclerosis on MRI (Hudak et al. 2004), a pathology in drug-resistant epilepsy that is highly amenable to epilepsy surgery. However, the challenge is that these patients often have other coexisting pathologies (Diaz-Arrastia et al. 2000) which tends to lower the success of epilepsy surgery in these patients (Dhamija et al. 2011). One of the key determinants of success in epilepsy surgery is the early detection of drug-resistant epilepsy and offering surgery in the early stages of the illness (Engel et al. 2012). The findings that we show associating the detections of lesions and functional connectivity abnormalities in the temporal lobe may be a manifestation of the underlying process of epileptogenesis that takes place in patients with PTE.

In this study, we explored the feasibility of predicting PTE using functional and structural imaging features, which consisted of fMRI connectivity, lesion volumes, and the ALEF in fMRI data. In particular, we assessed the performance of widely employed machine-learning algorithms in predicting PTE using these features. The aim was twofold: (1) to assess the feasibility of building predictive ML algorithms for PTE based on functional and structural brain features and (2) to leverage this data-driven framework to pinpoint discriminant brain features that may provide useful mechanistic insights into the clinical underpinnings of PTE.

Among the machine-learning models examined here, KSVM combined with a standard PCA approach for feature dimensionality reduction led to the highest prediction score. Additionally, our results suggest that combining all three feature types (connectivity, lesion, and ALFF data) leads to better prediction than only using one of the three types of features. The feasibility of successfully training a model to

discriminate PTE from non-PTE subjects demonstrates that complementary brain features extracted from multi-spectral MRI can collectively capture anatomo-functional alterations that underpin PTE. The ability of the ML approach to generalize to data from individuals that were not used in training the classifier (i.e., using cross-validation) indicates the feasibility of using the identified features to predict with a reasonable degree of accuracy whether a patient who suffers a traumatic brain injury is likely to go on to develop PTE or not. Our results show a maximum AUC of 0.78 using KSVM. Improvements in this value may result from the use of larger training sets, as we discuss below.

Although we employed several methods to compare the PTE and non-PTE groups, we observed reasonable consistency across the results. The results from the group difference analyses based on F-tests and the ML classifier results, as well as the feature importance maps (based on the SVM coefficients), provide converging evidence for alterations in temporal and occipital cortices, and to some extent in the cerebellum, in both functional and structural features. We note that the discrepancy between some of the structural and functional patterns observed in the right parietal regions may be due to the functional connectivity between parietal areas and epilepsy-related networks.

Furthermore, it is noteworthy that while the findings from lesion-based analysis were largely left-right symmetric, the ALFF-based analysis results showed a certain degree of asymmetry. To probe this further, we compared lesion volumes in left-hemisphere ROIs and in the corresponding right-hemisphere ROIs. This revealed that the left-right lesion volume differences were not significant for any of the ROIs. In the ALFF-based analysis, the region-wise results were largely symmetric, but in the left temporal and left parietal lobes, the p values approached significance. The p value in the ALFF analysis for the cerebellum also approached significance.

The AUC metric is a commonly used performance criterion in binary classification. While performance requirements vary across tasks and application domains, an AUC score of 0.7 is frequently used to indicate a minimally acceptable discrimination (Schummers et al. 2016; Steyerberg 2019; Swets 1988). However, a higher AUC is often necessary to stratify a significant portion of the population into high-risk or low-risk subjects. Schummers et al. (2016) suggested that to classify the majority of the population into a clinically distinct risk group (high or low risk), an AUC of 0.85 was needed. In our analysis, the highest performance (AUC=0.78) was obtained with the KSVM algorithm in a total sample size of 72 individuals (36 PTE and 36 non-PTE subjects). Due to the small study population, as a precaution, we verified that the AUCs were significantly better than the chance-level classifiers. To understand the impact of the number of subjects on the AUC, we repeated the ML analysis for different subsets of subjects (maintaining balanced sample sizes for PTE and non-PTE subjects). Figure 6 depicts the AUC's mean and variance based on stratified cross-validation as a function of the number of training subjects. Our results suggest that the AUC starts to increase monotonically after 26 subjects. A quadratically fit curve that extrapolates this trend is shown as a dotted red line. We fit a curve to the last 6

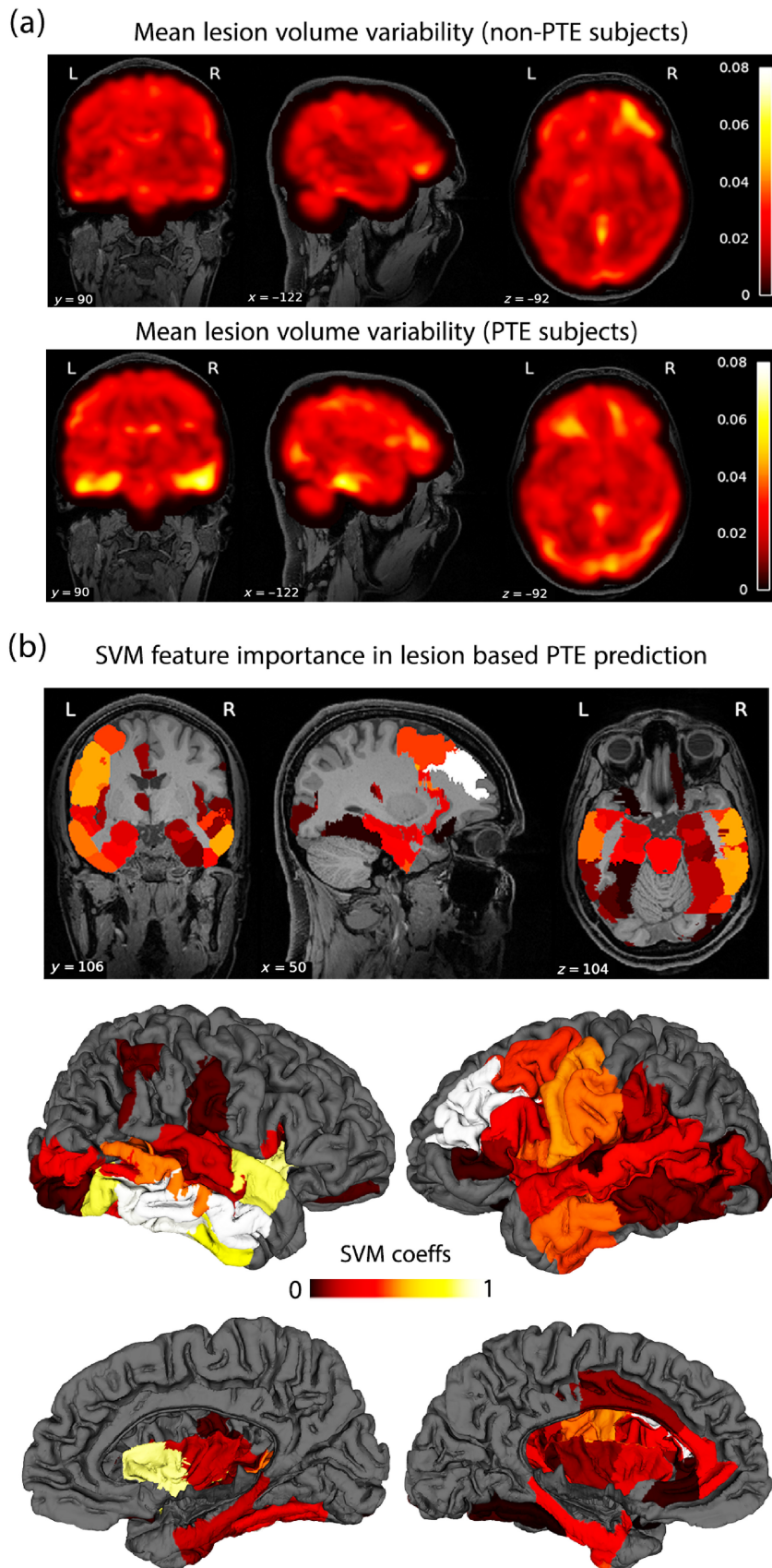


FIGURE 5 | (a) Brain-wide mean lesion volume variability is shown for non-PTE (upper row) and PTE subjects (lower row). (b) The feature importance map is shown as color-coded ROIs overlaid on the USCBrain atlas. Both cortical surface and volumetric ROIs are shown.

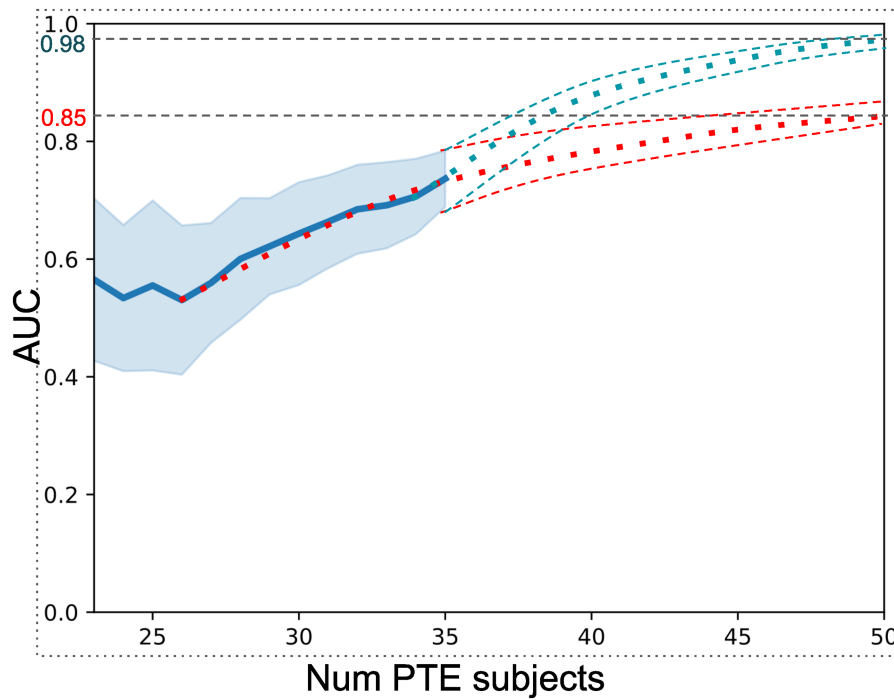


FIGURE 6 | Number of samples versus AUC resulting from KSVM (PCA) method. The blue curve shows the mean AUC and shaded areas indicate standard deviation in the leave-one out stratified cross-validation. Conservative (red) and optimistic (blue) extrapolations are shown as dotted curves.

data points to obtain an over-optimistic estimate of 0.98 AUC for 50 PTE subjects. By fitting the last 10 points we obtain a more conservative AUC value of 0.85 for 50 PTE subjects. Assuming a 15% prevalence of PTE in TBI subjects, this analysis shows that $N=300$ would yield the desired AUC with the existing algorithm. This is, of course, an attempt to extrapolate our results to outline a pragmatic and clinically relevant approach to using our method for the prediction of PTE. Of course, there are a number of unknown variables and factors that can influence this analysis. These include the heterogeneity of TBI and a wide range of properties of TBI patients (incl. demographics, types, the severity of injuries, treatment at the acute stage, etc.). In particular, the properties of the Maryland data used for this analysis can be quite different from those of other datasets.

4.1 | Limitations

Despite the encouraging and clinically relevant observations reported here, the PTE prediction method proposed is a first step that paves the way for more efficient and elaborate prediction approaches. Among relevant future steps, we believe that increasing the size of the training data and the addition of more features such as diffusion imaging data may lead to an improved AUC. Similarly, prediction is likely to benefit from incorporating non-imaging clinical data such as scores on the Glasgow Coma Scale (GCS), which classifies Traumatic Brain Injuries, alongside demographics and injury mechanisms. As noted earlier, this information was unfortunately not available in the public domain for the cohort we used in this study. Furthermore, including information on the type of epilepsy may turn out to be useful for training the ML models. This and other clinical information can also be used to further sub-group the clinical population. Another limitation of our study is its relatively small

population size ($N=72$). A larger study using the TrackTBI dataset might be possible in the future. The results from leave-one-out cross-validation show the relatively stable performance of the prediction methods. However, the AUC score may be further improved with a larger dataset.

5 | Conclusion

In this paper, we investigated the efficiency of functional and structural brain features as PTE biomarkers. Leveraging a machine-learning framework, we compared PTE prediction performance across an array of standard classifiers and a variety of brain features. The best results were obtained with KSVM, which is possibly partly due to the heterogeneity of the alterations in the PTE group around the mean feature. Our results using kernel-based methods show promising results. In both lesion and ALFF comparison studies, bilateral temporal lobes and cerebellum show significance. Moreover, there is potential involvement of the parietal and occipital lobes. Cross-sectional studies of children with chronic localization-related epilepsy (LRE) using traditional volumetric and voxel-based morphometry have revealed abnormalities in the cerebellum, frontal and temporal lobes, hippocampus, amygdala, and thalamus (Cormack et al. 2005; Daley et al. 2008; Guimaraes et al. 2007; Lawson et al. 1998, 2000, 1997; Tosun et al. 2011). The temporal lobe findings from our study further support this evidence.

Author Contributions

Haleh Akrami: conceptualization and study design, data analysis and interpretation, manuscript drafting and revision. **Wenhui Cui:** data acquisition, preprocessing, statistical analysis, and manuscript

drafting. **Paul E. Kim:** methodology development, software implementation, data visualization, manuscript review. **Christianne N. Heck:** supervision, funding acquisition, and critical review of the manuscript for important intellectual content. **Andrei Irimia:** manuscript drafting. **Karim Jerbi:** manuscript drafting, study design, and validation. **Dileep Nair:** validation of results, funding acquisition, and manuscript editing. **Richard M. Leahy:** project administration and manuscript drafting. **Anand A. Joshi:** project administration, validation of results, manuscript editing, and data analysis. All authors reviewed and approved the final version of the manuscript.

Acknowledgments

This work is supported by NIH grants: R01EB026299, R01NS074980, and DoD grants: W81XWH181061 and HT94252310149. Data used in the preparation of this article reside in the Department of Defense (DoD) and National Institutes of Health (NIH)-supported Federal Interagency Traumatic Brain Injury Research Informatics Systems (FITBIR) in FITBIR-STUDY 0000314 and FITBIR-STUDY 0000246. This manuscript reflects the authors' views and does not reflect the opinions or views of the DoD or the NIH.

Disclosure

The authors have nothing to report.

Conflicts of Interest

The authors declare no conflicts of interest.

Data Availability Statement

The data that support the findings of this study are openly available in FITBIR at <https://fitbir.nih.gov/>.

References

Agrawal, A., J. Timothy, L. Pandit, and M. Manju. 2006. "Post-Traumatic Epilepsy: An Overview." *Clinical Neurology and Neurosurgery* 108, no. 5: 433–439.

Akrami, H., A. Irimia, W. Cui, A. A. Joshi, and R. M. Leahy. 2021. "Prediction of Posttraumatic Epilepsy Using Machine Learning." In *Medical Imaging 2021: Biomedical Applications in Molecular, Structural, and Functional Imaging*, 11600, 424–430.

Akrami, H., A. A. Joshi, J. Li, S. Aydöre, and R. M. Leahy. 2020. "Brain Lesion Detection Using a Robust Variational Autoencoder and Transfer Learning." In *2020 IEEE 17th International Symposium on Biomedical Imaging (ISBI)*, 786–790.

Akrami, H., A. A. Joshi, J. Li, S. Aydore, and R. M. Leahy. 2022. "A Robust Variational Autoencoder Using Beta Divergence." *Knowledge-Based Systems* 238: 107886.

Akrami, H., R. Leahy, A. Irimia, P. Kim, C. Heck, and A. Joshi. 2022. "Neuroanatomic Markers of Posttraumatic Epilepsy Based on Mr Imaging and Machine Learning." *American Journal of Neuroradiology* 43, no. 3: 347–353.

Arslan, S., S. I. Ktena, A. Makropoulos, E. C. Robinson, D. Rueckert, and S. Parisot. 2018. "Human Brain Mapping: A Systematic Comparison of Parcellation Methods for the Human Cerebral Cortex." *NeuroImage* 170: 5–30.

Baud, M. O., J. K. Kleen, E. A. Mirro, et al. 2018. "Multi-Day Rhythms Modulate Seizure Risk in Epilepsy." *Nature Communications* 9, no. 1: 1–10.

Benjamini, Y., and Y. Hochberg. 1995. "Controlling the False Discovery Rate: A Practical and Powerful Approach to Multiple Testing." *Journal of the Royal Statistical Society: Series B: Methodological* 57, no. 1: 289–300. <https://doi.org/10.1111/j.2517-6161.1995.tb02031.x>.

Berg, J., F. Tagliaferri, and F. Servadei. 2005. "Cost of Trauma in Europe." *European Journal of Neurology* 12, no. Suppl 1: 85–90.

Breiman, L. 2001. "Random Forests." *Machine Learning* 45, no. 1: 5–32.

Burke, J., J. Gugger, K. Ding, J. A. Kim, B. Foreman, and J. K. Yue. 2021. "Association of Posttraumatic Epilepsy With 1-Year Outcomes After Traumatic Brain Injury." *JAMA Network Open* 4, no. 12: e2140191.

Bushnik, T., J. L. Cook, A. A. Yuzpe, S. Tough, and J. Collins. 2012. "Estimating the Prevalence of Infertility in Canada." *Human Reproduction* 27, no. 3: 738–746.

Chen, X., and E. Konukoglu. 2018. "Unsupervised Detection of Lesions in Brain Mri Using Constrained Adversarial Auto-Encoders." arXiv Preprint arXiv.

Collins, D. L., C. J. Holmes, T. M. Peters, and A. C. Evans. 1995. "Automatic 3-d Model-Based Neuroanatomical Segmentation." *Human Brain Mapping* 3, no. 3: 190–208.

Cormack, F., D. G. Gadian, F. Vargha-Khadem, J. H. Cross, A. Connelly, and T. Baldeweg. 2005. "Extra-Hippocampal Grey Matter Density Abnormalities in Paediatric Mesial Temporal Sclerosis." *NeuroImage* 27, no. 3: 635–643.

Cortes, C., and V. Vapnik. 1995. "Support-Vector Networks." *Machine Learning* 20, no. 3: 273–297.

Cox, R. W. 2012. "AFNI: What a Long Strange Trip it's Been." *NeuroImage* 62, no. 2: 743–747.

Cui, W., H. Akrami, G. Zhao, A. A. Joshi, and R. M. Leahy. 2023. "Meta Transfer of Self-Supervised Knowledge: Foundation Model in Action for Post-Traumatic Epilepsy Prediction." arXiv Preprint arXiv.

Daley, M., P. Siddarth, J. Levitt, et al. 2008. "Amygdala Volume and Psychopathology in Childhood Complex Partial Seizures." *Epilepsy & Behavior* 13, no. 1: 212–217.

D'Ambrosio, R., and E. Perucca. 2004. "Epilepsy After Head Injury." *Current Opinion in Neurology* 17, no. 6: 731–735.

Dennis, E. L., X. Hua, J. Villalon-Reina, L. M. Moran, C. Kernan, and T. Babikian. 2016. "Tensor-Based Morphometry Reveals Volumetric Deficits in Moderate/Severe Pediatric Traumatic Brain Injury." *Journal of Neurotrauma* 33, no. 9: 840–852.

Dhamija, R., B. D. Moseley, G. D. Cascino, and E. C. Wirrell. 2011. "A Population-Based Study of Long-Term Outcome of Epilepsy in Childhood With a Focal or Hemispheric Lesion on Neuroimaging." *Epilepsia* 52, no. 8: 1522–1526.

Diaz-Arrastia, R., M. A. Agostini, A. B. Frol, et al. 2000. "Neurophysiologic and Neuroradiologic Features of Intractable Epilepsy After Traumatic Brain Injury in Adults." *Archives of Neurology* 57, no. 11: 1611–1616.

Duda, R. O., P. E. Hart, and D. G. Stork. 2012. *Pattern Classification*. Hoboken, New Jersey: John Wiley & Sons.

Dunteman, G. H. 1989. *Principal Components Analysis*. California, USA: Sage.

Engel, J., M. P. McDermott, S. Wiebe, J. T. Langfitt, J. M. Stern, and S. Dewar. 2012. "Early Surgical Therapy for Drug-Resistant Temporal Lobe Epilepsy: A Randomized Trial." *JAMA* 307, no. 9: 922–930.

Engel, J., Jr., A. Pitkänen, J. A. Loeb, F. Edward Dudek, E. H. Bertram III, and A. J. Cole. 2013. "Epilepsy Biomarkers." *Epilepsia* 54: 61–69.

Fan, L., H. Li, J. Zhuo, Y. Zhang, J. Wang, and L. Chen. 2016. "The Human Brainnetome Atlas: A New Brain Atlas Based on Connectional Architecture." *Cerebral Cortex* 26, no. 8: 3508–3526.

Farbota, K. D., A. Sodhi, B. B. Bendlin, et al. 2012. "Longitudinal Volumetric Changes Following Traumatic Brain Injury: A Tensor-Based Morphometry Study." *Journal of the International Neuropsychological Society* 18, no. 6: 1006–1018.

- Fordington, S., and M. Manford. 2020. "A Review of Seizures and Epilepsy Following Traumatic Brain Injury." *Journal of Neurology* 267: 3105–3111.
- Frey, L. C. 2003. "Epidemiology of Posttraumatic Epilepsy: A Critical Review." *Epilepsia* 44: 11–17.
- Gale, S. D., L. Baxter, N. Roundy, and S. Johnson. 2005. "Traumatic Brain Injury and Grey Matter Concentration: A Preliminary Voxel Based Morphometry Study." *Journal of Neurology, Neurosurgery & Psychiatry* 76, no. 7: 984–988.
- Genovese, C. R., N. A. Lazar, and T. Nichols. 2002. "Thresholding of Statistical Maps in Functional Neuroimaging Using the False Discovery Rate." *NeuroImage* 15, no. 4: 870–878.
- Glasser, M. F., S. N. Sotiropoulos, J. A. Wilson, T. S. Coalson, B. Fischl, and J. L. Andersson. 2013. "The Minimal Preprocessing Pipelines for the Human Connectome Project." *NeuroImage* 80: 105–124.
- Guimaraes, C. A., L. Bonilha, R. C. Franzon, L. M. Li, F. Cendes, and M. M. Guerreiro. 2007. "Distribution of Regional Gray Matter Abnormalities in a Pediatric Population With Temporal Lobe Epilepsy and Correlation With Neuropsychological Performance." *Epilepsy & Behavior* 11, no. 4: 558–566.
- Gullapalli, R. P. 2011. "Investigation of Prognostic Ability of Novel Imaging Markers for Traumatic Brain Injury (Tbi)." USA: BALTIMORE UNIV MD.
- Hastie, T., R. Tibshirani, and J. Friedman. 2001. *The Elements of Statistical Learning*. New York, USA: Springer.
- Herman, S. T. 2002. "Epilepsy After Brain Insult: Targeting Epileptogenesis." *Neurology* 59, no. 9 suppl 5: S21–S26.
- Hudak, A. M., K. Trivedi, C. R. Harper, et al. 2004. "Evaluation of Seizure-Like Episodes in Survivors of Moderate and Severe Traumatic Brain Injury." *Journal of Head Trauma Rehabilitation* 19, no. 4: 290–295.
- Humphreys, I., R. L. Wood, C. J. Phillips, and S. Macey. 2013. "The Costs of Traumatic Brain Injury: A Literature Review." *ClinicoEconomics and Outcomes Research: CEOR* 5: 281.
- Immonen, R., I. Kharatishvili, O. Gröhn, and A. Pitkänen. 2013. "Mri Biomarkers for Post-Traumatic Epileptogenesis." *Journal of Neurotrauma* 30, no. 14: 1305–1309.
- Immonen, R. J., I. Kharatishvili, H. Gröhn, A. Pitkänen, and O. H. Gröhn. 2009. "Quantitative Mri Predicts Long-Term Structural and Functional Outcome After Experimental Traumatic Brain Injury." *NeuroImage* 45, no. 1: 1–9.
- Jenkinson, M., C. F. Beckmann, T. E. Behrens, M. W. Woolrich, and S. M. Smith. 2012. "FSL." *NeuroImage* 62, no. 2: 782–790.
- Joshi, A. A., S. Choi, Y. Liu, M. Chong, G. Sonkar, and J. Gonzalez-Martinez. 2022. "A Hybrid High-Resolution Anatomical Mri Atlas With Sub-Parcellation of Cortical Gyri Using Resting Fmri." *Journal of Neuroscience Methods* 374: 109566.
- Joshi, A. A., D. McCoy, M. Chong, et al. 2018. "BFP: BrainSuite fMRI Pipeline." Singapore.
- Joshi, A. A., D. W. Shattuck, P. M. Thompson, and R. M. Leahy. 2005. "A Framework for Registration, Statistical Characterization and Classification of Cortically Constrained Functional Imaging Data." In Biennial International Conference on Information Processing in Medical Imaging, 186–196.
- Joshi, A. A., D. W. Shattuck, P. M. Thompson, and R. M. Leahy. 2007. "Surface-Constrained Volumetric Brain Registration Using Harmonic Mappings." *IEEE Transactions on Medical Imaging* 26, no. 12: 1657–1669.
- Kim, J., B. Avants, S. Patel, et al. 2008. "Structural Consequences of Diffuse Traumatic Brain Injury: A Large Deformation Tensor-Based Morphometry Study." *NeuroImage* 39, no. 3: 1014–1026.
- Kingma, D. P., and M. Welling. 2013. "Auto-Encoding Variational Bayes." *arXiv Preprint arXiv*.
- Lawson, J. A., M. J. Cook, A. F. Bleasel, V. Nayanar, K. F. Morris, and A. M. Bye. 1997. "Quantitative Mri in Outpatient Childhood Epilepsy." *Epilepsia* 38, no. 12: 1289–1293.
- Lawson, J. A., W. Nguyen, A. F. Bleasel, et al. 1998. "Ilae-Defined Epilepsy Syndromes in Children: Correlation With Quantitative Mri." *Epilepsia* 39, no. 12: 1345–1349.
- Lawson, J. A., S. Vogrin, A. F. Bleasel, et al. 2000. "Predictors of Hippocampal, Cerebral, and Cerebellar Volume Reduction in Childhood Epilepsy." *Epilepsia* 41, no. 12: 1540–1545.
- Li, W., H. He, J. Lu, B. Lv, M. Li, and Z. Jin. 2009. Detection of Whole-Brain Abnormalities in Temporal Lobe Epilepsy Using Tensor-Based Morphometry With Dartel In Mippr 2009: Medical Imaging, Parallel Processing of Images, and Optimization Techniques, 7497.
- Li, X., N. C. Dvornek, Y. Zhou, J. Zhuang, P. Ventola, and J. S. Duncan. 2019. "Graph Neural Network for Interpreting Task-Fmri Biomarkers."
- Mann, H. B., and D. R. Whitney. 1947. "On a Test of Whether One of Two Random Variables Is Stochastically Larger Than the Other." *Annals of Mathematical Statistics* 18: 50–60.
- Meeuws, S., J. K. Yue, J. A. Huijben, et al. 2020. "Common Data Elements: Critical Assessment of Harmonization Between Current Multi-Center Traumatic Brain Injury Studies." *Journal of Neurotrauma* 37, no. 11: 1283–1290.
- Mo, J., Z. Liu, K. Sun, Y. Ma, W. Hu, and C. Zhang. 2019. "Automated Detection of Hippocampal Sclerosis Using Clinically Empirical and Radiomics Features." *Epilepsia* 60, no. 12: 2519–2529.
- Ng, S. Y., and A. Y. W. Lee. 2019. "Traumatic Brain Injuries: Pathophysiology and Potential Therapeutic Targets." *Frontiers in Cellular Neuroscience* 13: 528.
- Palacios, E. M., R. Sala-Llonch, C. Junque, et al. 2013. "Resting-State Functional Magnetic Resonance Imaging Activity and Connectivity and Cognitive Outcome in Traumatic Brain Injury." *JAMA Neurology* 70, no. 7: 845–851.
- Panayiotopoulos, C. P. 2005. "The Epilepsies: Seizures, Syndromes and Management." Bladon Medical Publishing, Oxfordshire (UK).
- Parikh, S., M. Koch, and R. K. Narayan. 2007. "Traumatic Brain Injury." *International Anesthesiology Clinics* 45, no. 3: 119–135.
- Pedersen, M., A. H. Omidvarnia, J. M. Walz, and G. D. Jackson. 2015. "Increased Segregation of Brain Networks in Focal Epilepsy: An Fmri Graph Theory Finding." *NeuroImage: Clinical* 8: 536–542.
- Perucca, E. 1998. "Pharmacoresistance in Epilepsy." *CNS Drugs* 10, no. 3: 171–179.
- Piccenna, L., G. Shears, and T. J. O'Brien. 2017. "Management of Post-Traumatic Epilepsy: An Evidence Review Over the Last 5 Years and Future Directions." *Epilepsia Open* 2, no. 2: 123–144.
- Pitkänen, A., and T. Bolqvadze. 2012. "Head Trauma and Epilepsy." In *Jasper's Basic Mechanisms of the Epilepsies [Internet]*. Oxford, United Kingdom: Oxford University Press.
- Pitkänen, A., W. Löscher, A. Vezzani, A. J. Becker, M. Simonato, and K. Lukasiuk. 2016. "Advances in the Development of Biomarkers for Epilepsy." *Lancet Neurology* 15, no. 8: 843–856.
- Potschka, H., and M. J. Brodie. 2012. "Pharmacoresistance." *Handbook of Clinical Neurology* 108: 741–757.
- Pustina, D., B. Avants, M. Sperling, et al. 2015. "Predicting the Laterality of Temporal Lobe Epilepsy From Pet, Mri, and Dti: A Multimodal Study." *NeuroImage: Clinical* 9: 20–31.
- Raymont, V., A. M. Salazar, R. Lipsky, D. Goldman, G. Tasick, and J. Grafman. 2010. "Correlates of Posttraumatic Epilepsy 35 Years Following Combat Brain Injury." *Neurology* 75, no. 3: 224–229.

- Ringnér, M. 2008. "What Is Principal Component Analysis?" *Nature Biotechnology* 26, no. 3: 303–304.
- Rocca, M. L., R. Garner, K. Jann, et al. 2019. "Machine Learning of Multimodal MRI to Predict the Development of Epileptic Seizures After Traumatic Brain Injury." openreview.net/forum?id=Bye0tkLNcV.
- Rolls, E. T., C.-C. Huang, C.-P. Lin, J. Feng, and M. Joliot. 2020. "Automated Anatomical Labelling Atlas 3." *NeuroImage* 206: 116189.
- Sackeim, H. A., P. Decina, S. Portnoy, P. Neeley, and S. Malitz. 1987. "Studies of Dosage, Seizure Threshold, and Seizure Duration in Ect." *Biological Psychiatry* 22, no. 3: 249–268.
- Schummers, L., K. P. Himes, L. M. Bodnar, and J. A. Hutcheon. 2016. "Predictor Characteristics Necessary for Building a Clinically Useful Risk Prediction Model: A Simulation Study." *BMC Medical Research Methodology* 16, no. 1: 1–10.
- Shattuck, D. W., and R. M. Leahy. 2002. "BrainSuite: An Automated Cortical Surface Identification Tool." *Medical Image Analysis* 6, no. 2: 129–142.
- Sidaros, A., A. Skimminge, M. G. Liptrot, et al. 2009. "Long-Term Global and Regional Brain Volume Changes Following Severe Traumatic Brain Injury: A Longitudinal Study With Clinical Correlates." *NeuroImage* 44, no. 1: 1–8.
- Sollee, J., L. Tang, A. B. Igiraneza, B. Xiao, H. X. Bai, and L. Yang. 2022. "Artificial Intelligence for Medical Image Analysis in Epilepsy." *Epilepsy Research* 182: 106861.
- Steyerberg, E. W. 2019. "Validation of Prediction Models." In *Clinical Prediction Models*, 329–344. New York, USA: Springer.
- Swartz, B. E., C. R. Houser, U. Tomiyasu, et al. 2006. "Hippocampal Cell Loss in Posttraumatic Human Epilepsy." *Epilepsia* 47, no. 8: 1373–1382.
- Swets, J. A. 1988. "Measuring the Accuracy of Diagnostic Systems." *Science* 240, no. 4857: 1285–1293.
- Tasker, R. C., C. H. Salmond, A. G. Westland, et al. 2005. "Head Circumference and Brain and Hippocampal Volume After Severe Traumatic Brain Injury in Childhood." *Pediatric Research* 58, no. 2: 302–308.
- Toloşi, L., and T. Lengauer. 2011. "Classification With Correlated Features: Unreliability of Feature Ranking and Solutions." *Bioinformatics* 27, no. 14: 1986–1994.
- Tosun, D., K. Dabbs, R. Caplan, et al. 2011. "Deformation-Based Morphometry of Prospective Neurodevelopmental Changes in New Onset Paediatric Epilepsy." *Brain* 134, no. 4: 1003–1014.
- Verellen, R. M., and J. E. Cavazos. 2010. "Post-Traumatic Epilepsy: An Overview." *Therapy* 7, no. 5: 527–531.
- Wang, P., J. Yang, Z. Yin, J. Duan, R. Zhang, and J. Sun. 2019. "Amplitude of Low-Frequency Fluctuation (Alff) may Be Associated With Cognitive Impairment in Schizophrenia: A Correlation Study." *BMC Psychiatry* 19, no. 1: 1–10.
- Wilde, E. A., E. D. Bigler, J. V. Hunter, et al. 2007. "Hippocampus, Amygdala, and Basal Ganglia Morphometrics in Children After Moderate-To-Severe Traumatic Brain Injury." *Developmental Medicine and Child Neurology* 49, no. 4: 294–299.
- Yamazoe, T., N. von Ellenrieder, H. M. Khoo, et al. 2019. "Widespread Interictal Epileptic Discharge More Likely Than Focal Discharges to Unveil the Seizure Onset Zone in Eeg-Fmri." *Clinical Neurophysiology* 130, no. 4: 429–438.
- Yount, R., K. A. Raschke, M. Biru, et al. 2002. "Traumatic Brain Injury and Atrophy of the Cingulate Gyrus." *Journal of Neuropsychiatry and Clinical Neurosciences* 14, no. 4: 416–423.
- Yue, J. K., M. J. Vassar, H. F. Lingsma, et al. 2013. "Transforming Research and Clinical Knowledge in Traumatic Brain Injury Pilot: Multicenter Implementation of the Common Data Elements for Traumatic Brain Injury." *Journal of Neurotrauma* 30, no. 22: 1831–1844.
- Zhang, J., K.-K. Ma, M.-H. Er, and V. Chong. 2004. "Tumor Segmentation From Magnetic Resonance Imaging by Learning via One-Class Support Vector Machine." In *International Workshop on Advanced Image Technology*, 207–211.
- Zhou, B., D. An, F. Xiao, R. Niu, W. Li, and W. Li. 2020. "Machine Learning for Detecting Mesial Temporal Lobe Epilepsy by Structural and Functional Neuroimaging." *Frontiers of Medicine* 14, no. 5: 630–641.
- Zhou, Y., M. P. Milham, Y. W. Lui, et al. 2012. "Default-Mode Network Disruption in Mild Traumatic Brain Injury." *Radiology* 265, no. 3: 882–892.
- Zuo, X.-N., A. Di Martino, C. Kelly, et al. 2010. "The Oscillating Brain: Complex and Reliable." *NeuroImage* 49, no. 2: 1432–1445.

Supporting Information

Additional supporting information can be found online in the Supporting Information section.